The hypothalamic link between arousal and sleep homeostasis in mice

Tomoko Yamagata[a], Martin C. Kahn[b], José Prius-Mengual[b], Elise Meijer[b], Merima Šabanović[c], Mathilde C. C. Guillaumin[a], Vincent van der Vinne[b], Yi-Ge Huang[b], Laura E. McKillop[b], Aarti Jagannath[a], Stuart N. Peirson[a], Edward O. Mann[b], Russell G. Foster[a,1], and Vladyslav V. Vyazovskiy[b,1]

[a]Sleep and Circadian Neuroscience Institute, Nuffield Department of Clinical Neurosciences, University of Oxford, Oxford OX1 3RE, United Kingdom; [b]Department of Physiology, Anatomy and Genetics, University of Oxford, Oxford OX1 3PT, United Kingdom; and [c]Department of Experimental Psychology, University of Oxford, Oxford OX2 6GG, United Kingdom

Edited by Joseph Takahashi, HHMI and Department of Neuroscience, The University of Texas Southwestern Medical Center, Dallas, TX; received January 25, 2021; accepted October 21, 2021

Sleep and wakefulness are not simple, homogenous all-or-none states but represent a spectrum of substates, distinguished by behavior, levels of arousal, and brain activity at the local and global levels. Until now, the role of the hypothalamic circuitry in sleep–wake control was studied primarily with respect to its contribution to rapid state transitions. In contrast, whether the hypothalamus modulates within-state dynamics (state "quality") and the functional significance thereof remains unexplored. Here, we show that photoactivation of inhibitory neurons in the lateral preoptic area (LPO) of the hypothalamus of adult male and female laboratory mice does not merely trigger awakening from sleep, but the resulting awake state is also characterized by an activated electroencephalogram (EEG) pattern, suggesting increased levels of arousal. This was associated with a faster build-up of sleep pressure, as reflected in higher EEG slow-wave activity (SWA) during subsequent sleep. In contrast, photoinhibition of inhibitory LPO neurons did not result in changes in vigilance states but was associated with persistently increased EEG SWA during spontaneous sleep. These findings suggest a role of the LPO in regulating arousal levels, which we propose as a key variable shaping the daily architecture of sleep–wake states.

sleep | hypothalamus | mice | sleep homeostasis | arousal

Interspecies variation in the daily amount of sleep is strongly influenced by genetic factors (1). However, individuals also possess a striking ability to adapt the timing and duration of wakefulness and sleep in response to a variety of intrinsic and extrinsic factors (2). Among the key regulators of "adaptive sleep architecture" are 1) homeostatic sleep need, 2) the endogenous circadian clock, and 3) the necessity to satisfy other physiological and behavioral needs such as feeding or the avoidance of danger (3–5). It is unknown how and in what form these numerous signals are integrated within the neural circuitry that generates the rapid and stable transitions between sleep and wake states.

Brain state switching has been the main focus of circuit-oriented sleep research for decades. Early studies identified the preoptic hypothalamus as a primary candidate for a hypothesized "key sleep center" (6–8), and subsequent studies have confirmed the existence of sleep-active neurons in the ventrolateral and median preoptic areas (VLPO and MPO) of the hypothalamus (9–11). Combined with the findings that orexin/hypocretin neurons are necessary to maintain wakefulness (12, 13), a model was proposed in which the sleep/wake-promoting circuitries function as a flip-flop switch (14). This model was able to account for rapid and complete transitions between sleep and wakefulness and preventing state instability (15) or the occurrence of mixed hybrid states of vigilance (16). Over the last decade, our knowledge of subcortical brain nuclei that control sleep has expanded steadily, leading to the identification of functional specialization within the sleep–wake controlling network and, in parallel, highlighting a previously underappreciated complexity (17–35).

A key question to emerge is how signals regulating sleep–wake architecture are represented and integrated in hypothalamic state-switching circuitries to ultimately maximize ecological fitness (36). Although sleep homeostasis has been considered an important factor influencing sleep/wake transitions (37–40), relatively few studies have addressed whether and how sleep–wake controlling brain areas overlap with those involved in homeostatic sleep regulation (26) or the underlying neurophysiological mechanisms (41–44). One recent study pointed to an important role of galanin neurons in the lateral preoptic hypothalamus, as was demonstrated through their selective ablation, which abolished the rebound of electroencephalogram (EEG) slow-wave activity (SWA; EEG power density between 0.5 to 4 Hz) after sleep deprivation (26). Other studies suggest that while homeostatic sleep pressure, reflected in SWA, builds up as a function of global wake duration, it is also locally regulated by specific activities during wakefulness (45, 46). The property of sleep and wake as brain states with flexible intensities on a global and local level suggests an additional complexity, which is difficult to reconcile with the existence of a single center solely responsible for complete sleep–wake switching (47). For example, there is evidence to suggest that wake "intensity" contributes to the build-up of global

Significance

Our current understanding of how sleep is regulated is based upon the model of sleep homeostasis, which defines a variable called Process S as a measure of sleep need, and a so-called "flip-flop" model of state switching, which builds on a notion of a mutually antagonistic relationship between subcortical sleep-promoting and wake-promoting circuits. The neurobiological substrates of the interaction between the sleep switch and Process S are unknown. Our study identifies a previously unrecognized role of hypothalamic circuitry in tuning within-state brain activity or levels of arousal, which in turn determine the homeostatic drive for sleep.

Author contributions: T.Y., A.J., S.N.P., E.O.M., R.G.F., and V.V.V. designed research; T.Y., M.C.K., J.P.-M., E.M., M.C.C.G., V.v.d.V., Y.-G.H., L.E.M., and E.O.M. performed research; T.Y. contributed new reagents/analytic tools; T.Y., M.C.K., M.Š., and E.O.M. analyzed data; and T.Y., M.C.K., M.C.C.G., V.v.d.V., L.E.M., and V.V.V. wrote the paper.

The authors declare no competing interest.

This article is a PNAS Direct Submission.

[1]To whom correspondence may be addressed. Email: vladyslav.vyazovskiy@dpag.ox.ac.uk or russell.foster@eye.ox.ac.uk.

This article contains supporting information online at http://www.pnas.org/lookup/suppl/doi:10.1073/pnas.2101580118/-/DCSupplemental.

Published December 13, 2021.

homeostatic sleep need (48–51), and the balance between intrinsic and extrinsic arousal-promoting and sleep-promoting signals ultimately determines the probability and degree of state switching (3, 52).

Here, we investigate the role of the hypothalamus in the bidirectional interactions between sleep–wake switching, arousal, and sleep homeostasis. Firstly, we applied optogenetic stimulation of glutamate decarboxylase 2 (GAD2) neurons in the lateral preoptic area (LPO) of mice (17) and found that photoactivation of the LPO during sleep led to rapid wake induction, but this effect was also observed when structures surrounding the LPO were stimulated. Unexpectedly, $GAD2^{LPO}$ neuronal stimulation did not merely trigger wakefulness, but the awake state produced by this stimulation was characterized by increased EEG theta activity—the established measure of arousal (53, 54). In turn, subsequent sleep was associated with increased levels of EEG SWA, indicative of higher homeostatic sleep pressure (45). In contrast, unilateral inhibition of $GAD2^{LPO}$ neurons decreased the drive for arousal, as was reflected in a persistent increase in nonrapid eye movement (NREM) EEG SWA across the day. In summary, our experiments demonstrate an important role of $GAD2^{LPO}$ neurons not only in the control of state transitions but also in linking arousal to sleep homeostasis. We find that the kinetics of the response to photoactivation and photoinhibition were different, and so they may arise from distinct mechanisms while converging on the dynamic modulation of arousal levels, ultimately shaping the daily architecture of sleep–wake states.

Results

Photoactivation of GAD2 Neurons in the Preoptic Hypothalamus Results in Wakefulness. We employed a previously described protocol to optically stimulate GAD2-expressing neurons in the LPO of the hypothalamus, which results in a rapid transition from sleep to wakefulness (17). To achieve the expression of channelrhodopsin-2 (ChR2), we injected adeno-associated virus (AAV) with cre-dependent expression of ChR2 fused with enhanced yellow fluorescent protein (AAV-DIO-ChR2-EYFP) and implanted an optic fiber targeting the preoptic hypothalamus in GAD2-cre mice ($n = 14$) (Fig. 1*A* and *SI Appendix*, Fig. S1 *A* and *B*). Subsequent histology confirmed virus expression in a broad area including the preoptic region of the hypothalamus and adjacent areas. Specifically, in 8 out of the 14 mice that expressed the virus, the tip of the optic fiber was located in the LPO (LPO group), while in the remaining six mice, the fiber tip was located within other neighboring hypothalamic areas posterior to the LPO (non-LPO group) (Fig. 1*B*) (55). Since optical stimulation may affect the

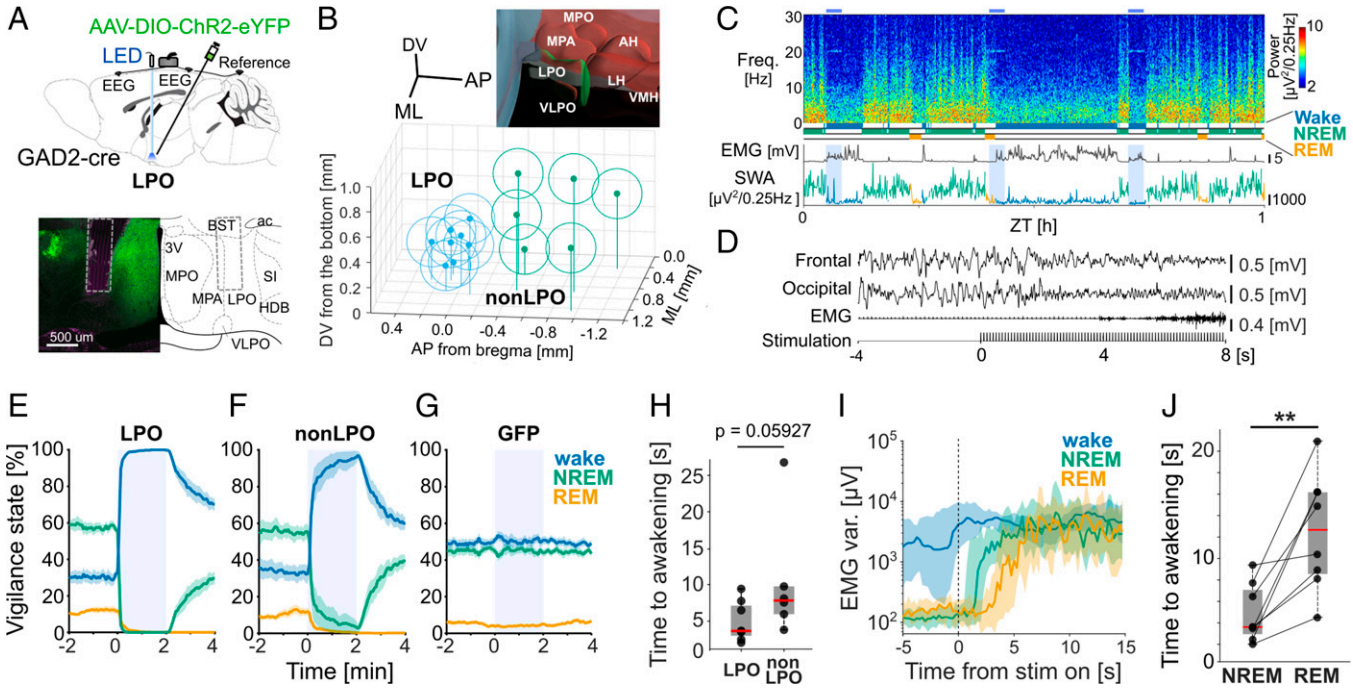

Fig. 1. Optical activation of GAD2 neurons in the LPO and surrounding hypothalamic regions induces rapid awakening. (*A*) (*Top*) Schematic diagram of the implant. (*Bottom*) Representative brain section from an animal in the LPO group and corresponding illustration from the mouse brain atlas (55). Dotted lines depict the optic fiber tip location. (*B*) Schematic of the optic fiber tip locations in all animals with ChR2 expression. The center of fiber tip is shown as a dot, and the stimulation coverage areas estimated based on a fiber diameter (400 µm) are shown as circles for individual animals. Blue, LPO group; green, non-LPO group. Top right inset shows the three-dimensional atlas of the hypothalamic area in the region of interest (ROI), constructed by the Allen Brain Explorer (beta). LPO is shown in green, and other hypothalamic nuclei in the ROI are shown in red. (*C*) Representative EEG spectrogram and the corresponding hypnogram, EMG, and EEG SWA. Blue shade, photostimulation. Freq, frequency. Color scale: spectral power in common logarithm values. Hypnogram and SWA are color coded according to vigilance state (blue, wake; green, NREM; yellow, REM). (*D*) EEG and EMG traces during a typical photostimulation trial in one individual animal. From top to bottom: frontal EEG, occipital EEG, EMG, and the timing of photostimulation. (*E*–*G*) Probability of wake, NREM sleep, and REM sleep before, during, and after a 2-min stimulation shown separately for the groups that received stimulation in the LPO area and outside of the LPO area (non-LPO) and GFP controls. Blue shade, photostimulation. Mean values ± SEM. (*H*) Latency to awakening. Data points represent individual mice. Box represents 25/75 percentiles, and median values are in red. The *P* value is calculated by nonparametric two-sided Wilcoxon signed-rank test. (*I*) Representative EMG variance profile (median ± 25/75 percentiles) averaged relative to the stimulation onset in one mouse. (*J*) Latency to awakening for stimulations delivered during spontaneous NREM sleep and REM sleep in the LPO. Data points represent individual mice, box represents 25/75 percentiles across mice, and red bar represents median. $^{**}P = 0.007$, two-sided Wilcoxon signed rank test. LPO, $n = 8$; non-LPO, $n = 6$; GFP controls, $n = 8$. 3V, third ventricle; ac, anterior commissure; AH, anterior hypothalamic area; AP, anteroposterior; BST, bed nucleus of stria terminalis; DV, dorsoventral; HDB, nucleus of the horizontal limb of the diagonal band; LH, lateral hypothalamic area; ML, mediolateral; MPA: medial preoptic area; SI, substantia innominata; VLPO, ventrolateral preoptic nucleus; VMH, ventromedial hypothalamic nucleus; ZT, Zeitgeber time.

animal's sleep and behavior because of local heating (56) or because of direct effects of light (57), we also analyzed a cohort of animals as a control group, which received the injection of AAV with cre-dependent expression of enhanced green fluorescent protein (AAV-DIO-EGFP) and were implanted with an optical fiber in the same area (GFP group). EEG and electromyogram (EMG) electrodes were also surgically implanted, as has been done previously (58), to enable identification of the sleep–wake state of the animal.

In the first set of experiments, we performed photoactivation in the same manner as used by Chung et al. (16), which consisted of delivering 2-min trains of light pulses at 10 Hz every 20 min throughout a full 24-h day, irrespective of the behavioral state (Fig. 1 *C* and *D* and *SI Appendix*, Fig. S1*C*). The 2-min period of stimulation was completely dominated by wakefulness in GAD2-ChR2 animals implanted in both LPO [Fig. 1*E*, Movie S1; wake probability during the second minute of photoactivation: stimulation (stim), 99.9 ± 0.1%; sham stimulation (sham), 45.3 ± 2.0%; $P < 0.0001$ in paired *t* test] and non-LPO locations (Fig. 1*F*; wake probability in stim: 99.1 ± 0.5%, sham: 50.8 ± 2.2%, $P < 0.0001$), but not in the GFP controls (Fig. 1*G*; wake probability in stim: 50.7 ± 2.35, sham: 48.1 ± 3.0%, $P > 0.1$). The average latency to awakening calculated based on EMG levels (Fig. 1*D* and *SI Appendix*, Fig. S1*D*) in the LPO group was on average 4.8 s (±0.94 SEM, $n = 8$) from the onset of stimulation and was slightly longer in the non-LPO group (10.3 ± 3.4 s, $n = 6$, Fig. 1*H*, $P = 0.059$, U = 61, two-tailed Wilcoxon rank-sum test). Interestingly, when stimulation was delivered during REM sleep, awakenings were delayed compared to NREM sleep in LPO (12.58 ± 1.9 s; $P = 0.007$; Fig. 1 *I* and *J*) and in the non-LPO group (*SI Appendix*, Fig. S1*E*). The latency to sleep upon cessation of stimulation was significantly longer if stimulation was performed when the animals were already awake (*SI Appendix*, Fig. S1*F*; wake: 9.05 ± 0.59 min, NREM: 4.47 ± 0.42 min, REM: 5.22 ± 0.70 min, $P < 0.0001$, one-way ANOVA), and longer in the non-LPO group as compared to the LPO group in the dark period (*SI Appendix*, Fig. S1*G*). Thus, the stimulation of hypothalamic GAD2 neurons during waking did not induce sleep but instead was followed by continued wakefulness.

Cellular Mechanism of GAD2^{LPO}-Mediated Awakening. Two recent observations on hypothalamic arousal circuitries may suggest potential cellular mechanisms underlying our observations. First, high-frequency stimulation causes some hypothalamic cells to enter a conduction block, which transforms optogenetic activation into de facto neuronal inhibition (25). Second, while the GAD2 promoter mainly targets inhibitory cells, it has been shown that GAD2 cells can also be excitatory (59).

To assess whether conduction block only occurred at high stimulation frequencies, 1-Hz, 2-Hz, and 5-Hz stimulation was sequentially applied to a subset of animals and compared to the awakening effect observed following stimulation frequencies of 10 Hz and 20 Hz (*SI Appendix*, Fig. S2 *A–C*). This showed that stimulation frequency had a pronounced effect on the probability to induce wakefulness (*SI Appendix*, Fig. S2*D*; repeated measures ANOVA [RM-ANOVA], $P < 0.01$, $n = 7$) and on the delay between stimulation onset and awakening (*SI Appendix*, Fig. S2*E*; RM-ANOVA, $P < 0.001$, $n = 7$). However, frequencies below 10 Hz did not appear to result in an inversion of the effect compared to stimulation at higher frequencies. Instead, the wake-promoting effect was stimulation-frequency dependent (*SI Appendix*, Fig. S2 *A–C*). In line with this, the latency to awakening was significantly influenced by the stimulation frequency (*SI Appendix*, Fig. S2*E*; $P < 0.05$ Wilcoxon signed-ranked test, $n = 7$). Similarly, the probability that an awakening occurred within 2 min of stimulation onset was 75.0% (±5.1) at 2 Hz, increased to 90.6% at 5 Hz, and peaked at 100% at 10 Hz (*SI Appendix*, Fig. S2*D*; $P < 0.05$ Wilcoxon signed-ranked test, $n = 7$). Thus, while the possibility that some of the neurons transfected by ChR2 in our study entered conduction block cannot be excluded, the absence of a qualitatively different response following high-frequency stimulation suggests that it is likely to affect only a minority of the cells. To support this conclusion, the galaninergic neurons in the LPO, for which conduction block was previously demonstrated, form only a small minority of LPO neurons (25).

The cellular substrate underlying the observed behavioral effects was further characterized by performing intracellular current clamp recordings from neurons in acute brain slices from GAD2^{LPO} mice. As this examination aimed to assess light responses in ChR2-expressing cells as well as their postsynaptic targets, cells in the LPO were targeted irrespective of ChR2 expression. As expected, a significant proportion of cells responded to negative current steps with hyperpolarization-induced sags and subsequent rebound low threshold spikes (LTSs) and hyperpolarization-induced inwards currents (47%, $n = 85$ cells; Fig. 2 *A*, *B*, and *F*). While almost all cells displayed spiking or subthreshold responses to light (90.6%), the delay between stimulation and response distinguished cells that were directly activated by ChR2 (<1 ms delay, 58%; Fig. 2*B*) from cells receiving synaptic inputs upon ChR2 activation. No differences were observed between LTS and non-LTS cells in the proportion of cells directly activated by ChR2 [Fig. 2*B*, *Bottom*; χ^2 (1, 3) = 1.22, $P = 0.75$, χ^2 test]. Next, we directly tested whether GAD2^{LPO} stimulation at 10 Hz is associated with conduction block and neuronal silencing. During 2 min of 10-Hz stimulation in putative ChR2-expressing cells, no signs of conduction block were found, and spike rates entrained to light pulses with high fidelity and independently of stimulation frequency (Fig. 2 *C* and *D*; $P = 0.70$, one-way ANOVA). Indeed, average spike rates during the stimulation period were slightly higher than the stimulation frequency (Fig. 2*E*). These results are in line with our behavioral observation that effects of in vivo stimulation at 10 Hz are qualitatively similar to those at lower frequencies.

Although the GAD2-Cre line was chosen to predominantly target ChR2 expression in inhibitory neurons, it has been suggested that GAD2 can also be expressed in excitatory neurons (59). To examine the postsynaptic effect of stimulating GAD2-ChR2 cells, the light responses to stimulation at 0.5 Hz were analyzed in putative non-ChR2 positive cells in the LPO (cells with subthreshold light responses and a delay to onset >1 ms). To distinguish GABAergic from glutamatergic inputs, light-evoked responses were recorded at different membrane potentials (Fig. 2*G*). At rest, non-ChR2 neurons responded to light with small depolarizing potentials, which turned into hyperpolarizing potentials at higher membrane potentials (Fig. 2*G*). This suggests that light induces a strong GABAergic response with a weaker glutamatergic component. In line with this, pharmacological inhibition of GABA-A receptors (10 μM bicuculline) abolished the hyperpolarizing potentials and unmasked excitatory responses (Fig. 2*H*; $n = 6$, $P = 0.02$, paired *t* test). Conversely, excitatory responses were sensitive to blocking ionotropic glutamate receptors with 10 μM 6-cyano-7-nitroquinoxaline-2,3-dione (CNQX), although this effect was weaker (Fig. 2*I*; $n = 6$, $P = 0.04$, paired *t* test). Strong inhibitory and weak excitatory currents suggested that GAD2^{LPO} stimulation had an overall inhibitory effect. This interpretation was tested by raising the membrane potential of ChR2-negative cells to promote spontaneous firing before delivering 2 min of light stimulation at 1, 2, 5, and 10 Hz, mimicking our in vivo protocol. The spontaneous firing rates in ChR2-negative cells did not significantly depend on stimulation frequency ($P = 0.43$, RM-ANOVA), although spontaneous firing rates were suppressed by stimulation [T(35) = −3.58, $P = 0.001$, one-sample *t* test against 0; Fig. 2*J*, yellow trace]. Note that our sample size was, however, likely too small to adequately resolve frequency dependency. Conversely, putative ChR2-positive cells

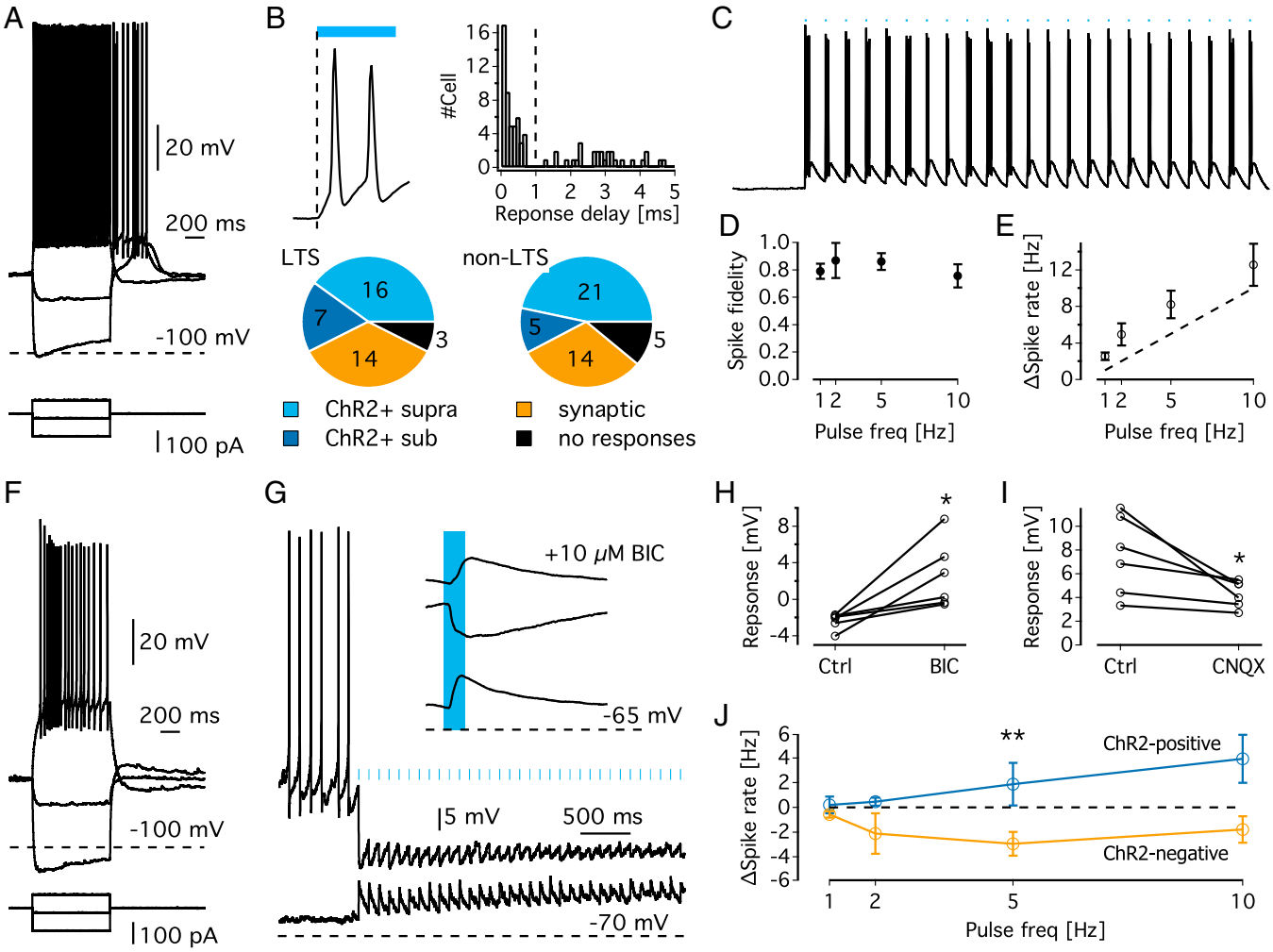

Fig. 2. Single-cell recordings in acute brain slices of GAD2^{LPO} mice. (*A*) Representative electrophysiological characteristics of an LTS neuron in the preoptic area. (*B*) (*Top left*) Example of a membrane potential (Vm) response to ChR2 activation in a putative ChR2-positive cell (magnification of the trace shown in panel *C*). Note that depolarization starts immediately upon the onset of illumination. (*Top right*) Histogram of delays between optical stimulation and Vm response showing a bimodal distribution; responses with delay <1 ms were classified as ChR2+, with delays >1 ms classified as synaptic responses. (*Bottom*) Classification of cells according to ChR2 response properties. (*C*) Example trace of a putative ChR2-positive cell responding to 10 Hz stimulation. (*D*) Spike fidelity of putative ChR2-positive neurons represented as the proportion of light pulses followed by a spike. (*E*) Relationship between stimulation frequency and mean spike rate during stimulation in putative ChR2-positive neurons. (*F*) Representative electrophysiological characteristics of a non-LTS neuron in the preoptic area. (*G*) Representative traces and average evoked potentials (*Top right*) of a ChR2-negative neuron, exhibiting depolarizing light responses at −70 mV (bottom trace and bottom average evoked potential) and hyperpolarizing responses at a slightly depolarized Vm (upper trace and middle in average evoked responses). The top average evoked potential shows the light response at a depolarized membrane potential in the presence of bicuculline. Note the unmasking of excitatory responses. (*H*) Change in average evoked responses (at depolarized Vm) in response to blocking of ionotropic GABA receptors with bicuculline. *$P = 0.02$, $t = 3.34$, paired t test. (*I*) Change in average evoked responses (at resting Vm) in response to blockage of ionotropic glutamate receptors with CNQX. *$P = 0.04$, $t = -2.78$, paired t test. (*J*) Changes in spontaneous spike rates (induced by injection of depolarizing currents) during 2 min of optical stimulation at 1, 2, 5, and 10 Hz. ** represents significant increase in spike rate in ChR2 group [$F(1,53) = 9.46$, $P = 0.003$] but no significant effect of stimulation frequency [$F(3,53) = 0.74$, $P = 0.53$] or interaction [$F(3,53) = 1.13$, $P = 0.35$; two-way ANOVA]. BIC, bicuculline.

increased their firing rates in the same experimental paradigm (Fig. 2*J*, blue trace). Thus, the most parsimonious interpretation of our experiments in vivo and in brain slices is that the effects of GAD2^{LPO} stimulation reported in this study are driven largely by activating inhibitory neurons and are unaffected by conduction block.

Stimulation of GAD2 Neurons Awakens Mice from Dexmedetomidine Sedation. To further characterize the wake-promoting effect of GAD2 neurons in preoptic hypothalamus, we performed photostimulation during sedation with dexmedetomidine (Dex), which is an alpha2-adrenergic receptor agonist and known to induce "deep sleep"–like EEG activity (*SI Appendix*, Fig. S3*A*) as well as a decrease of body temperature and metabolic rates (*SI Appendix*, Fig. S3 *B–D*) (20, 26). Stimulation was delivered at 10 Hz over a 2-min period every 15 min, and the initial and the late phases of Dex sedation were analyzed separately, corresponding to the first four stimulations (hour 0 to 1) and stimulations between 2 to 3 h from Dex injection, respectively. Within 5 min following the injection of Dex, the animals were sedated—immobile, typically lying outside of the nest in a prone position—and in all cases, the EEG was dominated by high-amplitude slow waves (*SI Appendix*, Fig. S3*A*) while peripheral body temperature and metabolic rate decreased concurrently (Fig. 3*A* and *SI Appendix*, Fig. S3 *B–D*). During the initial phase of sedation, a rapid awakening was observed in

both the LPO- and non-LPO–stimulated group (Fig. 3 *B* and *C*), while photostimulation was not effective in the GFP control animals (Fig. 3*B*). Since we never observed stimulation-induced awakenings in the control animals, the latency could not be calculated and so is not reported here. Interestingly, upon stimulation onset but before the animals woke up, a drop in EEG SWA relative to prestimulation levels was observed in the LPO group only (*SI Appendix*, Fig. S3 *E* and *F*). Furthermore, the latency to awakening from sedation tended to be shorter in the LPO group as compared to non-LPO–stimulated animals (median 36 s for LPO, 80 s for non-LPO; $P = 0.092$, Welch's t test; Fig. 3*C*). Notably, although the latency to awakening was still substantially higher during stimulation under sedation as compared to spontaneous NREM sleep (*SI Appendix*, Fig. S3*G*; NREM: 5.3 ± 1.6 s, SEM, Dex: 31.4 ± 5.5 s, $n = 6$, $P < 0.05$, two-tailed paired t test), the animals showed largely normal behaviors after awakening, including exploration of novel objects (Movie S2). Once the 2-min stimulation was terminated, the animals returned to a sedated state within a few minutes (Fig. 3*B*), and high-amplitude SWA was re-established (Fig. 3*A*). Unexpectedly, during late sedation—2 to 3 h after Dex injection, when the peripheral body temperature dropped to nearly room temperature and the EEG amplitude was very low—stimulation still resulted in rapid awakening (Fig. 3*C* and *SI Appendix*, Fig. S3*H*), and the latency to awakening was significantly shorter as compared to trials performed early after Dex injection ($P < 0.0021$, two-way ANOVA, factor "0 to 1 h versus 2 to 3 h," $P = 0.0021$; post hoc test, LPO: $P = 0.0273$, non-LPO: $P = 0.0174$).

Sleep/Wake History Does Not Influence the Latency to Awakening upon Stimulation. We next hypothesized that elevated levels of sleep pressure would decrease the probability of awakening upon photostimulation. To this end, mice were stimulated after a 4-h sleep deprivation (SD) or following an undisturbed period of sleep (Fig. 3*D*). As expected, SWA during NREM sleep in the 4-h recovery period after SD was higher than the SWA levels during the corresponding time period following undisturbed sleep (Fig. 3*E*). Thus, photostimulation during the sleep period after SD or after an undisturbed period of sleep are referred to as the "high-sleep pressure" (HSP), and "low-sleep pressure" (LSP) conditions, respectively. Unexpectedly, the animals still woke up almost immediately once stimulation was commenced under HSP (Fig. 3*F*), and the latency to awakening was indistinguishable between the HSP and LSP conditions (Fig. 3*G*; $P > 0.1$, two-sided Wilcoxon signed-rank test; *SI Appendix*, Fig. S4*A*). The absence of an influence of sleep pressure was surprising as the levels of SWA during NREM sleep following SD were ∼70% higher than those during baseline sleep (Fig. 3*E*). We further compared the latency to sleep from stimulation offset, but this was not significantly different between HSP and LSP (*SI Appendix*, Fig. S4*B*), although overall SWA remained high during HSP despite regular sleep interruption (*SI Appendix*, Fig. S4*C*). Together, these results show that activation of a broad population of inhibitory neurons in the hypothalamus induces waking irrespective of homeostatic sleep pressure, but LPO activation does not abolish accumulated sleep pressure.

Repeated GAD2 Photoactivation in LPO, but Not Outside LPO, Generates Excess Sleep Pressure. Wakefulness produced by photoactivation of GAD2 neurons typically outlasted stimulation both in the LPO and non-LPO regions by 4.69 ± 0.42 and 4.85 ± 0.54 min, respectively ($P = 0.82$, Welch's t test). Given that the mice spent most of the time during stimulation sessions awake and since a total of 72 stimulation sessions were delivered during the 24-h period, we expected to observe a significant sleep loss. Indeed, the amount of sleep during the stimulation day was lower than the corresponding values during a baseline day in both LPO mice (86.3 ± 3%) and non-LPO mice (86.4 ± 3.3%), but not in the GFP group (100.4 ± 5.6%, Fig. 4*A*; RM-ANOVA, $P = 0.035$, t tests against 100% for LPO: $P = 0.002$, $n = 8$, non-LPO: $P = 0.01$, $n = 6$, GFP: $P = 0.7$, $n = 8$). However, while the suppression of NREM sleep during stimulation occurred in both LPO and non-LPO groups (Fig. 4*B*) and the overall amount was similarly reduced during the light period (Fig. 4*A*), we observed that the deficit in NREM sleep at the end of the 24 h remained in the LPO-stimulated group only (*SI Appendix*, Fig. S5*A*). Furthermore, REM sleep was affected by stimulation to a greater extent than NREM sleep; the overall amount was reduced during the light period both in LPO and in non-LPO (Fig. 4*A* and *SI Appendix*, Fig. S5 *A* and *B*), but the proportion of REM sleep per total sleep time across 24 h was significantly reduced in the LPO group only (Fig. 4*A*; RM-ANOVA, $P = 0.012$, post hoc tests for LPO: $P = 0.048$, non-LPO: $P = 0.098$, GFP: $P = 0.067$). These observed changes in NREM and REM sleep amount are in line with an interpretation that, because the repeated photoactivation was invariably followed by NREM sleep first, REM sleep was especially restricted by our experimental paradigm.

Sleep loss is compensated for not only by an increase in sleep time but also by changes in sleep intensity, measured as the levels of EEG SWA. Strikingly, despite the frequent fragmentation of sleep, we noticed that NREM sleep between stimulation sessions was characterized by an increase in SWA in the LPO group both in the light and in the dark periods, which was not observed in the non-LPO group or GFP controls (Fig. 4 *C*–*E* and *SI Appendix*, Figs. S5*C* and S6 *C* and *D*). Since non-LPO and LPO mice lost a comparable amount of sleep during the light period but the non-LPO group partially recovered the loss during the subsequent dark phase, we next assessed how NREM sleep SWA was distributed over the full 24-h day. The time course of SWA across the day normally follows a U-shaped pattern, with high SWA at light onset and decreased SWA in the middle of the 24-h day (Fig. 4*F*). Unexpectedly, we found that this pattern was absent in the LPO group, which instead manifested, on average, a consistently elevated SWA, and in some individuals an increasing trend of SWA was present during the light phase (Fig. 4 *C* and *F*). This altered daily time course of SWA was not observed in the non-LPO or GFP control mice (Fig. 4*F*; two-way ANOVA, $P = 0.0065$; post hoc Sidak's multiple comparison test for LPO, $P = 0.0006$; non-LPO, $P > 0.9999$; GFP, $P = 0.9804$). This was particularly interesting since the daily distribution of the amount of wake and NREM was comparable between LPO and non-LPO mice (*SI Appendix*, Fig. S5*B*). Consistently, the increase in cumulative slow-wave energy (SWE) over the day in LPO mice was characterized by a steeper slope during the stimulation day compared to baseline or non-LPO mice (Fig. 4*G* and *SI Appendix*, Fig. S5*D*; two-way ANOVA, $P = 0.0406$ for interaction of factors). Taken together, these results demonstrate that stimulation of the GAD2 neurons in LPO does not merely result in increased wakefulness but that the induced wake state is characterized by a faster build-up or overall greater levels of sleep pressure needing to be compensated for.

Stimulation of GAD2-LPO Results in Elevated EEG Theta Activity during Waking, which Correlates with SWA during Sleep. Previous studies suggest that the build-up of sleep pressure depends on the type of wake behavior and not simply wake duration (48–50, 60, 61). Therefore, we hypothesized that LPO and non-LPO stimulation have differential effects on brain activity during wakefulness. To test this hypothesis, first EEG spectra were compared during wakefulness induced by stimulation with EEG spectra obtained after spontaneous awakenings during baseline. In both LPO and non-LPO mice, stimulation-induced awakenings were associated with decreased frontal EEG power in the slow-wave range [Fig. 5 *A* and *B*; general linear mixed model, $P < 0.001$, $F(97) = 6.3$ for main effect of frequency and

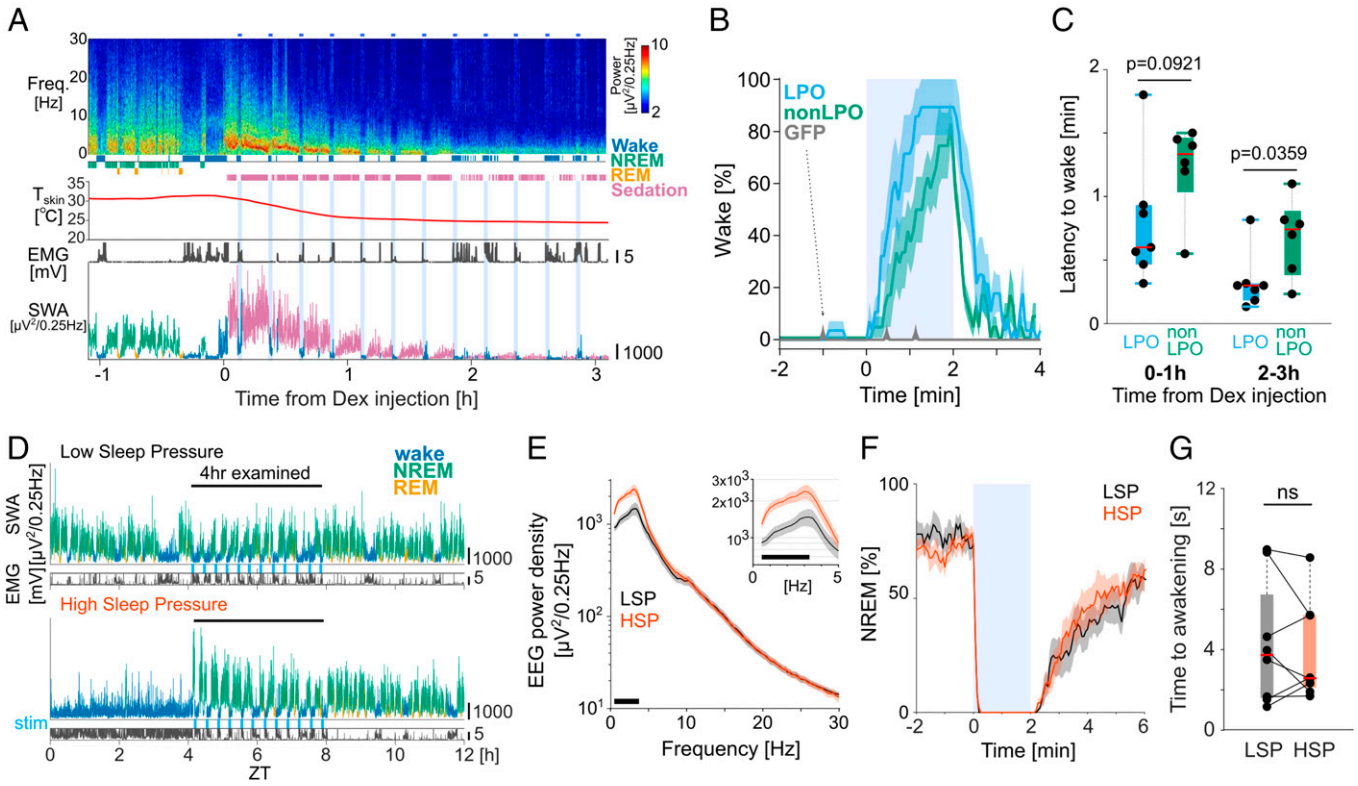

Fig. 3. Effects of photoactivation of GAD2^{LPO} neurons during sedation and HSP. (*A*) Representative frontal EEG spectrogram, hypnogram, peripheral body temperature, EMG, and SWA (EEG power between 0.5 and 4 Hz) color coded according to the state of vigilance, from one representative mouse, before and after Dex injection. Color scale: spectral power in common logarithm values. SWA is color coded according to vigilance state (blue, wake; green, NREM; yellow, REM; purple, sedation). (*B*) Percentage of time spent awake before, during, and after photostimulation (shaded area) during the first 1-h interval after Dex injection, averaged for LPO (n = 7), non-LPO (n = 6), and GFP (n = 8) animals. Mean values ± SEM. Note how in GFP animals (gray, arrow), the occurrence of wake-like states before or during stimulation was exceptionally rare. (*C*) Latency to awakening from sedation after the onset of stimulation calculated separately for the initial sedation (average of four stimulation sessions during the first hour after Dex injection) and during late sedation under hypothermia (average of four stimulations delivered between hours 2 to 3 after Dex injection) in LPO and non-LPO animals. Note that the latency to awakening from sedation in GFP is not shown because stimulation did not result in awakenings. Red bar, median; box: ±25/75 percentiles. *P* value, Welch's *t* test. (*D*) Representative 12-h profile of EEG SWA and EMG variance shown separately for "low" (*Top*) and "high" (*Bottom*) sleep pressure conditions. SWA is color coded according to vigilance state (blue, wake; green, NREM; yellow, REM). stim, photostimulation. (*E*) Mean EEG power spectra during the first 4 h of recovery sleep after SD and the corresponding baseline interval when sleep pressure was low (LSP). Mean values ± SEM. (*Inset*) Magnified spectra below 5 Hz. The black bar at the bottom of the figure denotes frequency bins in which the difference between LSP and HSP was significant in post hoc uncorrected Fisher's least significant difference (LSD) tests following a one-way ANOVA ($P < 0.05$). (*F*) Percentage of NREM sleep occurrence before, during, and after a 2-min photostimulation (shaded area) during HSP and LSP conditions. Mean values ± SEM. (*G*) Mean latency to awakening for stimulations delivered during HSP and LSP conditions. Data points represent individual mice, and red bar represents median across mice. ns, no significance in two-sided Wilcoxon signed-rank test. Box, ±25/75 percentiles. No. of animals used in *E*–*G*: LPO, n = 8.

$P > 0.5$ for group and frequency × group; see Fig. 5 for post hoc tests]. However, stimulation-induced wakefulness was also characterized by a greater increase in occipital EEG theta-frequency (6 to 9 Hz) power in the LPO group compared to the non-LPO group [Fig. 5 *A*–*C*; general linear mixed model, $P < 0.01$, $F(97) = 1.91$ for frequency × group; see Fig. 5*B* for post hoc rank-sum tests in frontal and occipital EEG]. Thus, photoactivation of the LPO area did not simply trigger an awakening, but the resulting wake state was also characterized by increased levels of arousal and alertness. We next hypothesized that such an altered wake state might account for the difference in sleep pressure between LPO and non-LPO mice (Fig. 4). In support of this hypothesis, across animals, a strong positive correlation was observed between the effects of stimulation on the occipital theta-frequency power (6 to 9 Hz) during wake and the effect of stimulation on SWA (0.5 to 4 Hz) during NREM sleep in the LPO group (Fig. 5*C*, *Lower*; Pearson's $R = 0.95$, $P = 0.0011$). Only nonsignificant and weak positive correlations were found in the occipital derivation in the non-LPO group ($R = 0.42$, $P > 0.1$; $P < 0.05$ for difference between LPO and non-LPO correlation coefficients), and no clear relationship was apparent in GFP animals ($R = -0.05$, $P > 0.1$). There was no significant correlation between the stimulation-induced changes in frontal SWA during wakefulness and SWA during NREM sleep in LPO, non-LPO, or GFP animals (Fig. 5*C*, *Upper*; Pearson's *R*: LPO, 0.49; non-LPO, 0.34: GFP, 0.06; all P values > 0.1), and the relationship was overall weaker for SWA as compared to theta activity in both LPO [$T(4) = 3.28$, $P < 0.05$ for difference between correlation coefficients] or combined LPO and non-LPO group [$T(10) = 3.06$, $P < 0.01$].

GAD2 Photoactivation during Wake in LPO Generates Excess Sleep Pressure. To directly address whether GAD2^{LPO} stimulation affects sleep homeostasis by modulating levels of arousal during wakefulness, we next delivered optostimulation while the animals were kept awake by novel objects (Fig. 5*D*; 20-s trains at 10 Hz, delivered every 2 min). We observed that EEG SWA during subsequent NREM sleep was increased in SD + LPO photoactivation condition compared to the no-stimulation condition (SD only), but not in GFP controls [Fig. 5*E*; LPO: $P = 0.0312$, $n = 6$, GFP: $P = 0.6875$, $n = 7$, Wilcoxon signed-rank

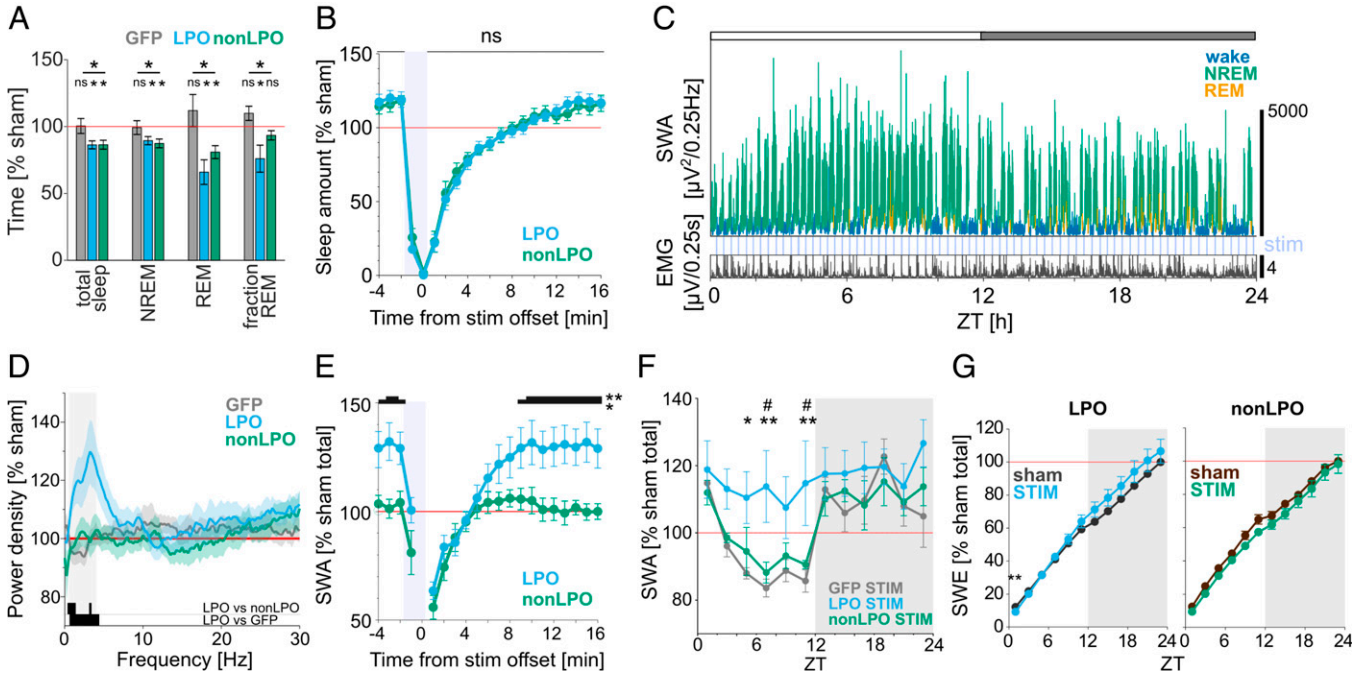

Fig. 4. Photoactivation induces a rebound of SWA during NREM sleep in GAD2^{LPO} but not in GAD2^{nonLPO} animals. (*A*) The effect of photostimulation on the total amount of vigilance states during the light period, shown as the percentage change relative to sham stimulation day. Stars above the lines indicate significant differences in RM-ANOVA, and stars and ns above plots indicate significance in *t* tests against 100%. *$P < 0.05$; ns, nonsignificant. Mean values ± SEM. (*B*) Amount of sleep during the 20-min window aligned to stimulation offset shown as percentage relative to the average sleep amount during sham stimulation day. All trials occurring during the light period are averaged for LPO and non-LPO animals. No significant difference was observed in sleep amount between the two groups using a two-way ANOVA ($P > 0.1$) and a post hoc uncorrected Fisher's LSD test. Mean values ± SEM. (*C*) Representative 24-h profile of EEG SWA and EMG in one individual animal that received stimulation to the LPO. SWA is plotted in 4-s resolution and is color coded according to vigilance state (green, NREM; blue, wake; yellow, REM). Note the progressive increase in SWA across the 12-h light period (indicated as a white bar on the top). (*D*) Relative EEG power density in NREM sleep shown for the 10-Hz 24-h stimulation condition during the light period compared to sham condition. Mean values ± SEM. Black bars at the bottom of the figure denote frequency bins in which the difference between experimental groups was significant ($P < 0.05$, unpaired *t* tests). Shaded area denotes the SWA frequency range (0.5 to 4 Hz). (*E*) Time course of EEG SWA over a 20-min window aligned to stimulation offset (time 0) during the light period. SWA is shown as a percentage of sham stimulation day SWA during the light period. *$P < 0.05$, **$P < 0.01$, post hoc uncorrected Fisher's LSD test following RM-ANOVA. Mean values ± SEM. (*F*) Time course of EEG SWA during NREM sleep across 24 h on the day with photostimulation. SWA is plotted in 2-h intervals and represented as percentage of average NREM SWA during sham stimulation day (mean values ± SEM; *or $^{\#}P < 0.05$, **$P < 0.01$, Tukey's multiple comparisons test after RM-ANOVA). *LPO versus GFP; $^{\#}$LPO versus non-LPO. (*G*) Cumulative EEG SWE across 24 h. Stars above plots indicate significance in multiple paired *t* tests. **$P < 0.01$. Comparison on the slope of SWE in the light period between LPO and non-LPO is shown in *SI Appendix*, Fig. S5*D*. Mean values ± SEM. No. of animals in *A*: LPO, $n = 8$; non-LPO, $n = 6$; GFP, $n = 8$. No. of animals in *D*–*F*: LPO, $n = 8$; non-LPO, $n = 6$; GFP, $n = 7$.

test for mean SWA (0.5 to 4 Hz); LPO versus GFP: $P = 0.0290$, unpaired *t* test for mean SWA]. There was a modest effect of photoactivation on the amount of waking and sleep following the end of SD, mostly reflected in increased wakefulness during the first 30 min after the animals were left undisturbed, which dissipated quickly (*SI Appendix*, Fig. S7). To examine whether the photoactivation-induced prolonged wakefulness after SD is directly responsible for the subsequent SWA increase, we calculated a correlation between the difference in total wake amount between the two conditions and corresponding SWA increase. Contrary to our hypothesis, there was no meaningful relationship observed (*SI Appendix*, Fig. S7*D*), suggesting that the difference in SWA during recovery sleep after GAD2^{LPO} activation is more likely accounted for by the change in the level of arousal (wake "quality") than wake duration.

To further assess whether prolonged photoactivation could induce further increases in brain activity during wakefulness or subsequent sleep, a subset of animals was exposed to an intense prolonged stimulation at 10 Hz for a 1-h interval starting either at light or dark onset (*SI Appendix*, Fig. S8). Unexpectedly, despite the animals being behaviorally awake, with brain activity and EMG indicating an unequivocal wake state, three out of four animals showed a marked decrease in peripheral body temperature (*SI Appendix*, Fig. S8*E*), which in one case outlasted the stimulation period by ∼4 h (*SI Appendix*, Fig. S8*B*).

Repeated GAD2 Photoinhibition Decreases Wakefulness and Arousal. Finally, we set out to investigate whether photoinhibition of GAD2 neurons in the LPO area results in changes in sleep–wake architecture and sleep intensity. Specifically, we expected that if photoactivation of these neurons increases arousal drive, which in turn is associated with increased sleep pressure, the results of suppressing the activity of inhibitory neurons in the LPO area should lead to reduced arousal. To this end, we undertook an experiment in which green light-emitting diode (LED) stimulation (550 nm, 18.8 to 24.0 mW at fiber tip) was applied to the LPO area in Arch-expressing mice ($n = 6$) and GFP controls ($n = 4$) (Fig. 6*A*). First, to examine the effect of stimulation on awake state and subsequent sleep, 2-min continuous stimulations with ramp down at stimulation offset were applied every 5 min during SD, as we did in the photoactivation experiment (Fig. 5*D*). The intensity of photostimulation was ramped down for ∼30 seconds prior to stimulation offset to prevent the burst activity at the end of the pulse to minimize bursting excitation of the neurons (62). Stimulation was stopped 10 min before the end of the 2-h SD, and in total,

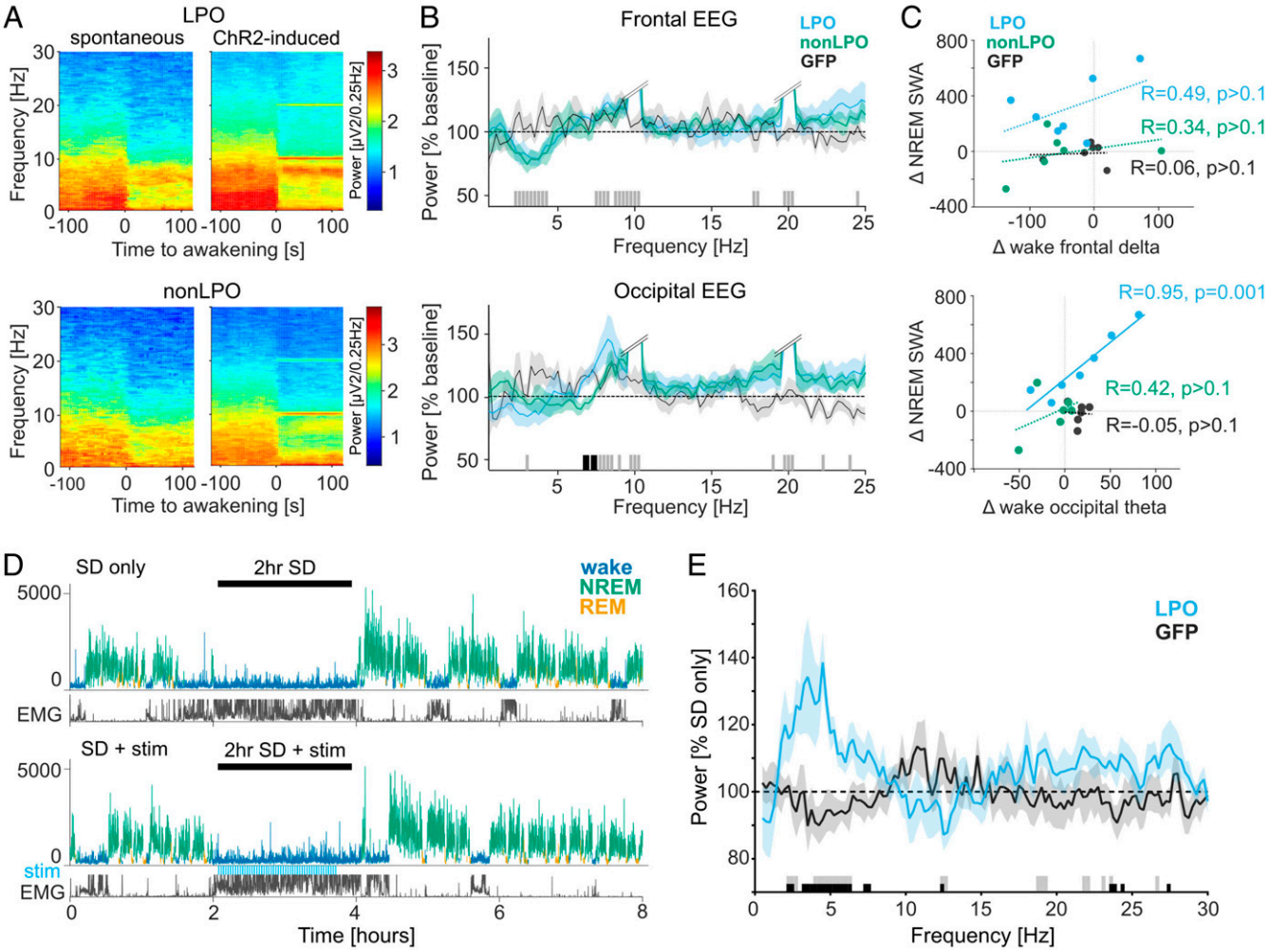

Fig. 5. Effects of LPO and non-LPO photoactivation on wakefulness and subsequent sleep. (*A*) Average wake-EEG spectrograms recorded from the occipital derivation of representative mice during spontaneous awakenings on a baseline day and during awakenings induced by photoactivation (*Top*: LPO, *Bottom*: non-LPO). Time 0 corresponds to the onset of waking. Color scale: spectral power in common logarithm values. (*B*) Average EEG spectral power density during photoactivation-induced awakenings expressed as a percentage of power during spontaneous awakenings during baseline. Bars at the bottom indicate significant differences ($P < 0.05$) in post hoc rank-sum tests following general linear mixed model; black, significant differences between LPO and non-LPO groups; gray, no significant differences between LPO and non-LPO groups but LPO and non-LPO groups combined are significantly different from 100%. Double slash: the cutoff for stimulation-induced artifacts at around 10 Hz and 20 Hz, from the frequency with steep increase in power, until the frequency with steep decrease. (*C*) Correlation between stimulation-associated differences in wake SWA and NREM SWA (*Top*) and in wake theta-frequency (6 to 9 Hz) power and NREM SWA (*Bottom*). *R*: Pearson's correlation coefficients, with corresponding *P* values. Note that only the correlation between wake theta-frequency power and NREM SWA in LPO group is statistically significant. (*D*) Representative hypnograms illustrating the experimental design for stimulation during SD. (*Top*) 2-h SD without stimulation (SD only). (*Bottom*) 2-h SD combined with photostimulation, shown as blue bars "stim." SWA plotted for 4-s epochs is color coded according to the state of vigilance. *y* axis in $\mu V^2/0.25$ Hz. (*E*) Effect of stimulation during wakefulness on EEG spectra during subsequent NREM sleep. The EEG power after SD + stim is calculated over the first 2 h of recovery sleep and represented as percent of "SD only" condition in the LPO and GFP animals. Bars at the bottom denote frequency bins in which the EEG power was significantly affected by stimulation ($P < 0.05$, *t* test); black, significant between GFP and LPO; gray, significant against 100% in LPO. No. of animals used in *B* and *C*: LPO, $n = 7$; non-LPO, $n = 6$; GFP, $n = 6$. No. of animals used in *D* and *E*: LPO, $n = 6$; GFP, $n = 7$.

the animals received 22 stimulation sessions over the 2-h period of continuous wakefulness. We observed only minor changes in the EEG during SD + stimulation as compared to SD only (Fig. 6 *B* and *C*), and, as could be expected, subsequent sleep did not differ between conditions. We hypothesized that relatively weak unilateral photoinhibition during SD is not sufficiently strong to override high levels of arousal in animals continuously provided with novel objects and engaged in exploratory behavior.

To address whether the effects of photoinhibition manifest in undisturbed animals not stimulated with novel objects, we next performed repeated stimulation over 24 h, which consisted of 5-min continuous pulses delivered every 30 min, irrespective of the state of vigilance, with a jitter of 10%. In total, 48 stimulations were delivered. No immediate effect of inhibition on state switching was observed (Fig. 6*E* and *SI Appendix*, Fig. S9*A*), and no change in total sleep and NREM sleep amount in the light period were found, while REM sleep amount was slightly reduced (Fig. 6*F*). In contrast, EEG spectral power during NREM sleep was characterized by higher levels of SWA (Fig. 6*G* and *SI Appendix*, Fig. S9*B*). In contrast to photoactivation (Fig. 4*F*), the time course of SWA during the day with photoinhibition was entirely normal (*SI Appendix*, Fig. S9*C*). We surmise that the persistent increase in SWA in this case is due to an overall attenuation of arousal drive rather than due to a progressive accrual of sleep debt. By the end of 24 h, SWE, which is a composite metric of sleep time and intensity, was ~20% higher in Arch-expressing

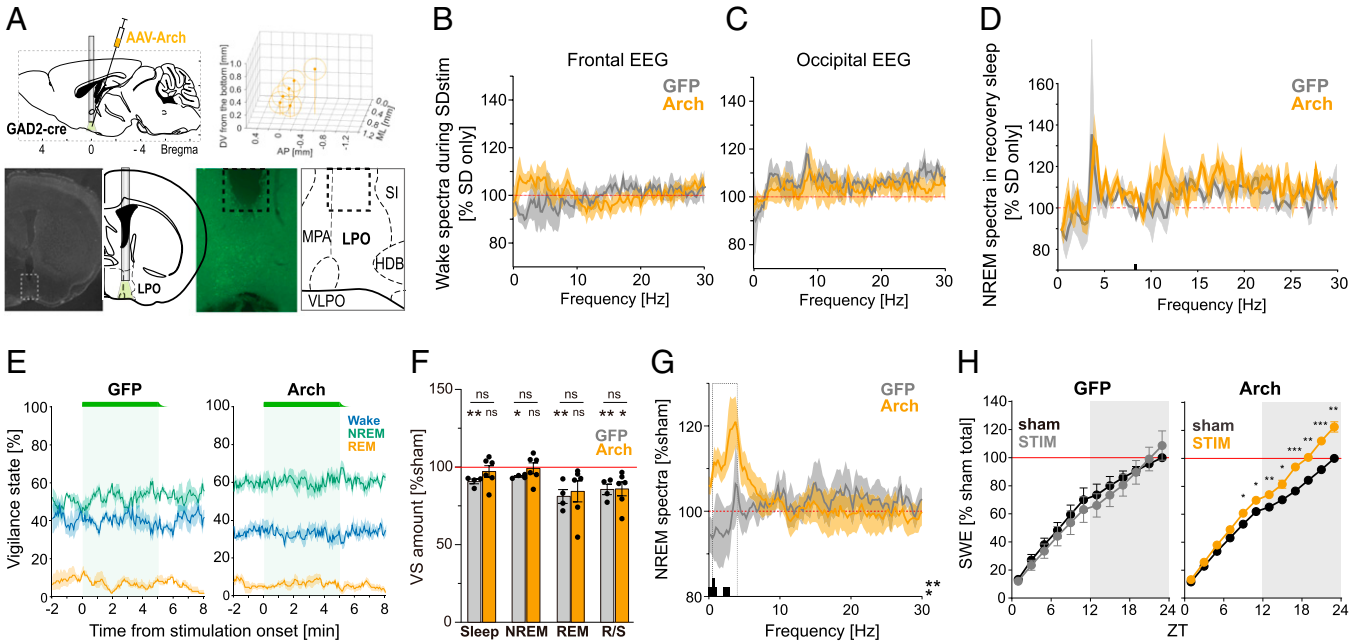

Fig. 6. Optical inhibition of GAD2^{LPO} neurons does not alter sleep pressure accumulation during SD but increases SWA and SWE when delivered during spontaneous sleep-wake states. (*A*) Representative histology from an animal with Arch expression in LPO used for optical inhibition. (*Top left*) Schematics of optical inhibition experiments. (*Top right*) Schematic of the optic fiber tip locations in all animals with Arch expression. The center of each fiber tip is shown as a dot, and the stimulation coverage areas estimated based on a fiber diameter (400 μm) are shown as circles for individual animals. (*Bottom left*) DAPI image and corresponding atlas (55) with implant schematics. Dotted square corresponds to the right panels. (*Bottom right*) fluorescence image of the squared area in the left panel and the corresponding atlas (Bregma = 0.02). Dotted lines depict the lesion from the implanted optic fiber. (*B* and *C*) Average 2-h wake spectra during SD + stimulation relative to 2-h SD-only condition for frontal EEG (*B*) and occipital EEG (*C*) in Arch and GFP control animals (n = 6 and n = 4, respectively; mean values ± SEM). (*D*) Effect of stimulation during SD on EEG spectra during subsequent NREM sleep. The EEG power after SD + stimulation is calculated over the first 2 h of recovery sleep and represented as percentage of the SD-only condition. Bars at the bottom denote frequency bins in which the EEG power was significantly affected by stimulation ($P < 0.05$). (*E*) Probability of wake, NREM and REM sleep before, during and after 5-min photoinhibition (shown as a green bar and shaded area) shown separately for the GFP controls and Arch group. Note the right end of the green bars reflecting the light ramp down. Mean values ± SEM. (*F*) The effect of photoinhibition on the total amount of vigilance states during the light period, shown as the percentage change relative to sham stimulation day. ns above lines indicates no difference in unpaired t test. Stars and ns above plots indicate significance levels in one-sample t tests against 100%. *$P < 0.05$, **$P < 0.01$. Mean values ± SEM. (*G*) Average EEG power spectra during NREM sleep on the day with photoinhibition shown as percentage of baseline day. Mean values ± SEM. Bars below the curves depict frequency bins in which EEG power was significantly different between GFP and Arch animals ($P < 0.05$). (*H*) Cumulative EEG SWE in NREM sleep across 24 h shown separately for GFP and Arch animals during sham and stim conditions. Stars above plots indicate significance in multiple paired t tests. *$P < 0.05$, **$P <$ 0.01, ***$P < 0.01$. Comparison on the slope of SWE in the light period between LPO and non-LPO is shown in *SI Appendix*, Fig. S9*D*.

animals, which was significantly higher than during sham stimulation condition or in GFP control animals (Fig. 6*H* and *SI Appendix*, Fig. S9*D*).

Discussion

The current study reports that photoactivation of inhibitory neurons in the lateral preoptic area of the hypothalamus does not simply trigger a transition from sleep to wakefulness but also increases the EEG indices of arousal. In turn, heightened arousal during the wake state is associated with a greater increase in sleep SWA, suggesting that the LPO not only controls global state switching but also contributes to the modulation of within-state dynamics of brain activity and homeostatic sleep drive. Photoinhibition of the same neurons further supported this notion, as it persistently decreased arousal levels without switching global state. These findings suggest that arousal level, above and beyond the duration of wakefulness, is an important parameter that contributes to the rate of accumulation of sleep need. Based on these findings, we propose adding a qualitative dimension to the influential model of sleep–wake control (37), which can be best represented as an in-built "switch with a spring." We posit that when wakefulness is especially intense, the "spring" becomes more compressed. As a result, once wakefulness ends, a stronger sleep rebound follows to release the "pressure."

Our observation of rapid awakening upon the start of GAD2^{LPO} photoactivation confirms earlier findings (17) and is consistent with the notion that only subsets of preoptic neurons are sleep active or sleep promoting (25, 63). Previous studies sometimes tacitly assumed that the same hypothalamic areas are implicated in both sleep promotion and sleep homeostasis. An alternative possibility is that sleep propensity may be enhanced if some of the strong wake-promoting areas are inhibited, consistent with the idea that sleep represents a default state of a neural network or the whole organism (46, 64). Therefore, even if accumulation of sleep need, in some form, occurs globally (51, 52, 65–74), it is likely that state switching is initiated from a relatively limited set of brain circuits, which have the capacity to integrate sleep–wake history–related signals with other ecological and homeostatic demands. While the biological substrate of global sleep homeostasis remains unclear, the question of which brain areas are involved in encoding the time spent awake or asleep seems tractable (41, 50, 51).

Interestingly, our data suggest that while photoactivation of LPO and non-LPO resulted in a comparable sleep loss, only LPO stimulation generates the enhanced sleep pressure manifesting as increased SWA during subsequent sleep. Furthermore, only LPO stimulation resulted in an increase in the EEG theta-frequency activity, an established marker of behavioral arousal and alertness (49, 54, 75–77), during induced awakenings. In addition, the

observed latency to awakening was longer when stimulation was delivered during REM sleep compared to NREM sleep. These observations argue against the possibility that our stimulation protocol was unphysiological or unspecific. Consistent with the observation that the build-up of sleep pressure is especially prominent during theta-dominant wakefulness, we observed that the increase in EEG theta activity during LPO stimulation correlated strongly with the increase in SWA during subsequent sleep, while photoactivation of GAD2^{LPO} neurons during spontaneous wakefulness led to a further increase in subsequent sleep intensity.

An acknowledged limitation of the approach we used is that we likely targeted a heterogeneous population of neurons, as the hypothalamus harbors many different cell types (35, 78). We would like to stress that it remains unclear how fine the spatial resolution should be in stimulation experiments such as ours, to obtain meaningful insights into cerebral substrates of global control of sleep and wakefulness. More relevant is that our chosen approach may have resulted in an activation of circuitries not directly, or not exclusively, related to sleep–wake control. For instance, LPO is adjacent to the lateral hypothalamus circuits, which contain GABAergic neurons that promote a wide range of functions, from reward-seeking behaviors to feeding (79–81). Moreover, the preoptic area of the hypothalamus contains inhibitory neurons involved in parental behaviors and various homeostatic processes such as thermoregulation and fluid homeostasis (82–84). Importantly, the LPO receives inputs from several limbic areas including the septum, subiculum, infralimbic cortex, amygdala, and the brainstem (85, 86), which can relay salient or aversive signals and therefore can function as an alarm system in response to important physiological drives or threats. In addition, a large population of GAD2 neurons in the LPO project to the parietal cortex and frontal cortex (17, 87), and it has been shown that selective photoactivation of prefrontally projecting preoptic GAD2 neurons modestly, but significantly, promotes wakefulness (17). Thus, the connectivity of the LPO, and particularly its inhibitory neurons, supports the view that this area plays a central role in integrating essential physiological drives linked to the regulation of arousal.

Our dexmedetomidine experiments showed that activation of GABAergic neurons in the hypothalamus under deep sedation is sufficient to produce arousal, consistent with the observations that sleep-active GAD neurons express α2A-adrenergic receptors and that selective ablation of galaninergic neurons in the LPO diminishes the effects of dexmedetomidine (26). Once again, LPO stimulation in sedated animals was more efficient in producing wakefulness and increasing cortical activation as compared to non-LPO stimulation. Surprisingly, animals showed largely normal wake behavior when stimulated during sedation, even though their peripheral body temperature was reduced to values close to room temperature. Our finding that continuous intense stimulation of the LPO can produce sustained wakefulness and hypothermia at the same time is intriguing and adds further complexity to the links between vigilance state regulation and temperature control (25, 26, 84, 88).

To further test the hypothesis that the LPO area of the hypothalamus contributes to changes in the global levels of arousal, we performed loss-of-function experiments, achieved by unilateral photoinhibition of GAD2^{LPO} neurons with LEDs that had sufficiently high light intensity for eArch3.0 photostimulation. Interestingly, we found that photoinhibition in active, alert animals during SD did not result in prominent changes in wake EEG, in contrast to photoactivation of the same neurons. Not surprisingly, this therefore did not lead to any changes in subsequent sleep. However, when photoinhibition was delivered in undisturbed animals during spontaneous wake and sleep, this resulted in reduced levels of arousal, as manifested in persistently enhanced sleep SWA.

Taken together with optical activation experiments, we speculate on the role of these neurons as follows. When the population of GAD2^{LPO} neurons is spontaneously active, which may be driven indirectly by external stimuli through inputs from other brain areas, such as hypocretin/orexin, noradrenaline, or cortical/striatal neurons (17, 41, 89, 90), the animals engage in wakefulness characterized by increased levels of activity and arousal, and this leads to a subsequent increase in sleep intensity (49, 61). This is increased further in already awake animals if the activity of these neurons is artificially enhanced by optostimulation, while rapid awakening occurs when stimulation is delivered during sleep. In contrast, a relatively weak selective unilateral inhibition imposed on GAD2^{LPO} neurons during SD does not lead to any effects because their reduced activity is compensated by strong unspecific environmental stimuli, which effectively drive other arousal-promoting neuronal populations (19). However, continuous inhibition of GAD2^{LPO} neurons during baseline in the absence of strong external stimulation, while not resulting in immediate state transitions, is ultimately sleep promoting. This is reflected in persistently reduced levels of arousal, i.e., associated with deeper sleep, as characterized by elevated SWA.

In conclusion, our study demonstrates that the LPO of the hypothalamus is not merely involved in global sleep/wake transitions but plays a more nuanced role in linking levels of arousal, within-state dynamics, and sleep homeostasis. Our data illustrate the important role of the hypothalamus in vigilance state control and provide an important step toward a more holistic characterization of the neural substrates of sleep regulation.

Materials and Methods

For detailed methods, see *SI Appendix*. All experimental procedures were performed under UK Home Office Project License #P828B64BC in accordance with Animal (Scientific Procedures) Act 1986 and the guideline of the University of Oxford. Male and female Gad2-IRES-Cre mice (Jackson Laboratory 019022; B6N.Cg-*Gad2*$^{tm2(cre)Zjh}$/J) were used in this study. Viruses were obtained from UNC vector core. Chronic EEG and EMG recordings were obtained and analyzed as previously described (58). Virus injection and optical stimulation were targeted to the lateral preoptic area of the hypothalamus. Electrophysiological data were acquired with a Tucker-Davis Technologies recording system. SD was performed as previously described (75). In sedation experiments, Dex was diluted with saline and injected subcutaneously (100 μg/kg). Skin temperature was measured using infrared thermal imaging cameras Optris Xi 70 and Xi 80 (Optris GmbH) (91). Metabolic rates were measured using indirect calorimetry with CaloBox (PhenoSys). At the end of the experiment, mice were deeply anesthetized and transcardially perfused with 0.1 M phosphate-buffered saline (PBS), followed by 4% paraformaldehyde in PBS for subsequent histology to confirm virus expression and optic fiber location. Acute slice preparation and recording was performed as described previously (92). Statistical analyses were performed in MATLAB (The MathWorks), SPSS (IBM), and GraphPad Prism (GraphPad).

Data Availability. Data reported in this study are included in the article, *SI Appendix*, and/or in *Dataset S1*. The code generated during this study were deposited by T.Y. on GitHub (November 27, 2021) and can be accessed via https://github.com/TomokoYamagataw/Yamagata_PNAS_HypLinkArousalSleepHomeostasis. Supplementary materials and methods, figures S1 to S9, table S1, and legends for movies S1 to S2 can be found in the *SI Appendix*.

ACKNOWLEDGMENTS. We thank Prof. Denis Burdakov, Dr. Christin Kosse, Dr. Hannah Alfonsa, and Dr. Adam Packer for advice on experiments, data analysis, and interpretation and Prof. Gerhard Heldmaier for advice on using CaloBox. We thank members of V.V.V.'s laboratory and SCNi for help with experiments and for comments on the manuscript. This work was supported by Wellcome Trust Senior Investigator Award (106174/Z/14/Z, to R.G.F.), Wellcome Trust Strategic Award (098461/Z/12/Z, to R.G.F.), John Fell Oxford University Press Research Fund Grant (131/032, to V.V.V.), FP7-PEOPLE-CIG (PCIG11-GA-2012-322050, to V.V.V.), Medical Research Council (MR/L003635/1 and MR/S01134X/1, to V.V.V.), Royal Society (RG120466, to V.V.V.), Naito Foundation (Grant for Studying Overseas, to T.Y.), and Uehara Memorial Foundation (Postdoctoral Fellowships for Research Abroad, to T.Y.).

1. R. Allada, J. M. Siegel, Unearthing the phylogenetic roots of sleep. *Curr. Biol.* **18**, R670–R679 (2008).
2. G. Ungurean, J. van der Meij, N. C. Rattenborg, J. A. Lesku, Evolution and plasticity of sleep. *Curr. Opin. Physiol.* **15**, 111–119 (2020).
3. A. Eban-Rothschild, L. Appelbaum, L. de Lecea, Neuronal mechanisms for sleep/wake regulation and modulatory drive. *Neuropsychopharmacology* **43**, 937–952 (2018).
4. T. Korotkova, A. Ponomarenko, To eat? To sleep? To run? Coordination of innate behaviors by lateral hypothalamus. *Neuroforum* **23**, 45 (2017).
5. B. Collins *et al.*, Circadian VIPergic neurons of the suprachiasmatic nuclei sculpt the sleep-wake cycle. *Neuron* **108**, 486–499.e5 (2020).
6. C. V. Economo, Sleep as a problem of localization. *J. Nerv. Ment. Dis.* **71**, 249–259 (1930).
7. W. J. Nauta, Hypothalamic regulation of sleep in rats; an experimental study. *J. Neurophysiol.* **9**, 285–316 (1946).
8. M. Sallanon *et al.*, Long-lasting insomnia induced by preoptic neuron lesions and its transient reversal by muscimol injection into the posterior hypothalamus in the cat. *Neuroscience* **32**, 669–683 (1989).
9. R. Szymusiak, D. McGinty, Hypothalamic regulation of sleep and arousal. *Ann. N. Y. Acad. Sci.* **1129**, 275–286 (2008).
10. D. McGinty, R. Szymusiak, Brain structures and mechanisms involved in the generation of NREM sleep: Focus on the preoptic hypothalamus. *Sleep Med. Rev.* **5**, 323–342 (2001).
11. J. E. Sherin, P. J. Shiromani, R. W. McCarley, C. B. Saper, Activation of ventrolateral preoptic neurons during sleep. *Science* **271**, 216–219 (1996).
12. R. M. Chemelli *et al.*, Narcolepsy in orexin knockout mice: Molecular genetics of sleep regulation. *Cell* **98**, 437–451 (1999).
13. L. Lin *et al.*, The sleep disorder canine narcolepsy is caused by a mutation in the hypocretin (orexin) receptor 2 gene. *Cell* **98**, 365–376 (1999).
14. C. B. Saper, T. C. Chou, T. E. Scammell, The sleep switch: Hypothalamic control of sleep and wakefulness. *Trends Neurosci.* **24**, 726–731 (2001).
15. T. Mochizuki *et al.*, Behavioral state instability in orexin knock-out mice. *J. Neurosci.* **24**, 6291–6300 (2004).
16. M. W. Mahowald, M. A. Cramer Bornemann, C. H. Schenck, State dissociation, human behavior, and consciousness. *Curr. Top. Med. Chem.* **11**, 2392–2402 (2011).
17. S. Chung *et al.*, Identification of preoptic sleep neurons using retrograde labelling and gene profiling. *Nature* **545**, 477–481 (2017).
18. D. Liu *et al.*, A common hub for sleep and motor control in the substantia nigra. *Science* **367**, 440–445 (2020).
19. D. Liu, Y. Dan, A motor theory of sleep-wake control: Arousal-action circuit. *Annu. Rev. Neurosci.* **42**, 27–46 (2019).
20. Z. Zhang *et al.*, Neuronal ensembles sufficient for recovery sleep and the sedative actions of α2 adrenergic agonists. *Nat. Neurosci.* **18**, 553–561 (2015).
21. Y. Oishi *et al.*, Slow-wave sleep is controlled by a subset of nucleus accumbens core neurons in mice. *Nat. Commun.* **8**, 734 (2017).
22. P. Zhong *et al.*, Control of non-REM sleep by midbrain neurotensinergic neurons. *Neuron* **104**, 795–809.e6 (2019).
23. F. Weber *et al.*, Regulation of REM and Non-REM sleep by periaqueductal GABAergic neurons. *Nat. Commun.* **9**, 354 (2018).
24. C. G. Herrera *et al.*, Hypothalamic feedforward inhibition of thalamocortical network controls arousal and consciousness. *Nat. Neurosci.* **19**, 290–298 (2016).
25. D. Kroeger *et al.*, Galanin neurons in the ventrolateral preoptic area promote sleep and heat loss in mice. *Nat. Commun.* **9**, 4129 (2018).
26. Y. Ma *et al.*, Galanin neurons unite sleep homeostasis and α2-adrenergic sedation. *Curr. Biol.* **29**, 3315–3322.e3 (2019).
27. S. Chowdhury *et al.*, GABA neurons in the ventral tegmental area regulate non-rapid eye movement sleep in mice. *eLife* **8**, e44928 (2019).
28. S. Chowdhury *et al.*, Dissociating orexin-dependent and -independent functions of orexin neurons using novel Orexin-Flp knock-in mice. *eLife* **8**, e44927 (2019).
29. X. Yu *et al.*, GABA and glutamate neurons in the VTA regulate sleep and wakefulness. *Nat. Neurosci.* **22**, 106–119 (2019).
30. F. Mátyás *et al.*, A highly collateralized thalamic cell type with arousal-predicting activity serves as a key hub for graded state transitions in the forebrain. *Nat. Neurosci.* **21**, 1551–1562 (2018).
31. Y. Hayashi *et al.*, Cells of a common developmental origin regulate REM/non-REM sleep and wakefulness in mice. *Science* **350**, 957–961 (2015).
32. H. Hayat *et al.*, Locus coeruleus norepinephrine activity mediates sensory-evoked awakenings from sleep. *Sci. Adv.* **6**, eaaz4232 (2020).
33. G. Oikonomou *et al.*, The serotonergic raphe promote sleep in zebrafish and mice. *Neuron* **103**, 686–701.e8 (2019).
34. A. Fujita *et al.*, Hypothalamic tuberomammillary nucleus neurons: Electrophysiological diversity and essential role in arousal stability. *J. Neurosci.* **37**, 9574–9592 (2017).
35. L. F. Jiang-Xie *et al.*, A common neuroendocrine substrate for diverse general anesthetics and sleep. *Neuron* **102**, 1053–1065.e4 (2019).
36. A. Eban-Rothschild, W. J. Giardino, L. de Lecea, To sleep or not to sleep: Neuronal and ecological insights. *Curr. Opin. Neurobiol.* **44**, 132–138 (2017).
37. C. B. Saper, P. M. Fuller, N. P. Pedersen, J. Lu, T. E. Scammell, Sleep state switching. *Neuron* **68**, 1023–1042 (2010).
38. M. E. Carter, A. Adamantidis, H. Ohtsu, K. Deisseroth, L. de Lecea, Sleep homeostasis modulates hypocretin-mediated sleep-to-wake transitions. *J. Neurosci.* **29**, 10939–10949 (2009).
39. M. A. Alam, S. Kumar, D. McGinty, M. N. Alam, R. Szymusiak, Neuronal activity in the preoptic hypothalamus during sleep deprivation and recovery sleep. *J. Neurophysiol.* **111**, 287–299 (2014).
40. C. Cirelli, M. Pompeiano, G. Tononi, Sleep deprivation and c-fos expression in the rat brain. *J. Sleep Res.* **4**, 92–106 (1995).
41. L. B. Krone *et al.*, A role for the cortex in sleep-wake regulation. *Nat. Neurosci.* **24**, 1210–1215 (2021).
42. S. R. Morairty *et al.*, A role for cortical nNOS/NK1 neurons in coupling homeostatic sleep drive to EEG slow wave activity. *Proc. Natl. Acad. Sci. U.S.A.* **110**, 20272–20277 (2013).
43. W. Peng *et al.*, Regulation of sleep homeostasis mediator adenosine by basal forebrain glutamatergic neurons. *Science* **369**, eabb0556 (2020).
44. T. C. Gent, M. Bandarabadi, C. G. Herrera, A. R. Adamantidis, Thalamic dual control of sleep and wakefulness. *Nat. Neurosci.* **21**, 974–984 (2018).
45. V. V. Vyazovskiy, K. D. Harris, Sleep and the single neuron: The role of global slow oscillations in individual cell rest. *Nat. Rev. Neurosci.* **14**, 443–451 (2013).
46. J. M. Krueger, Y. H. Huang, D. M. Rector, D. J. Buysse, Sleep: A synchrony of cell activity-driven small network states. *Eur. J. Neurosci.* **38**, 2199–2209 (2013).
47. R. Szymusiak, Hypothalamic versus neocortical control of sleep. *Curr. Opin. Pulm. Med.* **16**, 530–535 (2010).
48. S. P. Fisher *et al.*, Stereotypic wheel running decreases cortical activity in mice. *Nat. Commun.* **7**, 13138 (2016).
49. A. Vassalli, P. Franken, Hypocretin (orexin) is critical in sustaining theta/gamma-rich waking behaviors that drive sleep need. *Proc. Natl. Acad. Sci. U.S.A.* **114**, E5464–E5473 (2017).
50. C. W. Thomas, M. C. C. Guillaumin, L. E. McKillop, P. Achermann, V. V. Vyazovskiy, Global sleep homeostasis reflects temporally and spatially integrated local cortical neuronal activity. *eLife* **9**, e54148 (2020).
51. S. Reichert, O. Pavón Arocas, J. Rihel, The neuropeptide galanin is required for homeostatic rebound sleep following increased neuronal activity. *Neuron* **104**, 370–384.e5 (2019).
52. M. Lazarus, Y. Oishi, T. E. Bjorness, R. W. Greene, Gating and the need for sleep: Dissociable effects of adenosine A_1 and A_{2A} receptors. *Front. Neurosci.* **13**, 740 (2019).
53. M. J. McGinley *et al.*, Waking state: Rapid variations modulate neural and behavioral responses. *Neuron* **87**, 1143–1161 (2015).
54. I. R. Kemp, B. R. Kaada, The relation of hippocampal theta activity to arousal, attentive behaviour and somato-motor movements in unrestrained cats. *Brain Res.* **95**, 323–342 (1975).
55. G. Paxinos, K. B. J. Franklin, *The Mouse Brain in Stereotaxic Coordinates* (Academic Press, San Diego, ed. 2, 2001).
56. S. F. Owen, M. H. Liu, A. C. Kreitzer, Thermal constraints on in vivo optogenetic manipulations. *Nat. Neurosci.* **22**, 1061–1065 (2019).
57. K. M. Tyssowski, J. M. Gray, Blue light increases neuronal activity-regulated gene expression in the absence of optogenetic proteins. *eNeuro* **6**, ENEURO.0085-19.2019 (2019).
58. M. C. C. Guillaumin *et al.*, Cortical region-specific sleep homeostasis in mice: Effects of time of day and waking experience. *Sleep (Basel)* **41**, zsy079 (2018).
59. J. R. Moffitt *et al.*, Molecular, spatial, and functional single-cell profiling of the hypothalamic preoptic region. *Science* **362**, eaau5324 (2018).
60. A. Suzuki, C. M. Sinton, R. W. Greene, M. Yanagisawa, Behavioral and biochemical dissociation of arousal and homeostatic sleep need influenced by prior wakeful experience in mice. *Proc. Natl. Acad. Sci. U.S.A.* **110**, 10288–10293 (2013).
61. L. Milinski *et al.*, Waking experience modulates sleep need in mice. *BMC Biol.* **19**, 65 (2021).
62. M. Mahn, M. Prigge, S. Ron, R. Levy, O. Yizhar, Biophysical constraints of optogenetic inhibition at presynaptic terminals. *Nat. Neurosci.* **19**, 554–556 (2016).
63. M. Modirrousta, L. Mainville, B. E. Jones, Gabaergic neurons with alpha2-adrenergic receptors in basal forebrain and preoptic area express c-Fos during sleep. *Neuroscience* **129**, 803–810 (2004).
64. M. Bandarabadi, A. Vassalli, M. Tafti, Sleep as a default state of cortical and subcortical networks. *Curr. Opin. Physiol.* **15**, 60–67 (2020).
65. S. B. Noya *et al.*, The forebrain synaptic transcriptome is organized by clocks but its proteome is driven by sleep. *Science* **366**, eaav2642 (2019).
66. F. Brüning *et al.*, Sleep-wake cycles drive daily dynamics of synaptic phosphorylation. *Science* **366**, eaav3617 (2019).
67. S. Shi, H. R. Ueda, Ca^{2+}-dependent hyperpolarization pathways in sleep homeostasis and mental disorders. *BioEssays* **40**, 1700105 (2018).
68. F. Tatsuki *et al.*, Involvement of Ca(2+)-dependent hyperpolarization in sleep duration in mammals. *Neuron* **90**, 70–85 (2016).
69. T. Honda *et al.*, A single phosphorylation site of SIK3 regulates daily sleep amounts and sleep need in mice. *Proc. Natl. Acad. Sci. U.S.A.* **115**, 10458–10463 (2018).
70. C. M. Muheim *et al.*, Dynamic- and frequency-specific regulation of sleep oscillations by cortical potassium channels. *Curr. Biol.* **29**, 2983–2992.e3 (2019).
71. J. A. Williams, N. Naidoo, Sleep and cellular stress. *Curr. Opin. Physiol.* **15**, 104–110 (2020).
72. M. C. D. Bridi *et al.*, Daily oscillation of the excitation-inhibition balance in visual cortical circuits. *Neuron* **105**, 621–629.e4 (2020).
73. A. Varshavsky, On the cause of sleep: Protein fragments, the concept of sentinels, and links to epilepsy. *Proc. Natl. Acad. Sci. U.S.A.* **116**, 10773–10782 (2019).
74. A. Vaccaro *et al.*, Sleep loss can cause death through accumulation of reactive oxygen species in the gut. *Cell* **181**, 1307–1328.e15 (2020).

75. V. V. Vyazovskiy, I. Tobler, Theta activity in the waking EEG is a marker of sleep propensity in the rat. *Brain Res.* **1050**, 64–71 (2005).
76. R. Kramis, C. H. Vanderwolf, B. H. Bland, Two types of hippocampal rhythmical slow activity in both the rabbit and the rat: Relations to behavior and effects of atropine, diethyl ether, urethane, and pentobarbital. *Exp. Neurol.* **49**, 58–85 (1975).
77. J. Hubbard *et al.*, Dissecting and modeling photic and melanopsin effects to predict sleep disturbances induced by irregular light exposure in mice. *Proc. Natl. Acad. Sci. U.S.A.* **118**, e2017364118 (2021).
78. R. Chen, X. Wu, L. Jiang, Y. Zhang, Single-cell RNA-Seq reveals hypothalamic cell diversity. *Cell Rep.* **18**, 3227–3241 (2017).
79. N. Goldstein *et al.*, Hypothalamic neurons that regulate feeding can influence sleep/wake states based on homeostatic need. *Curr. Biol.* **28**, 3736–3747.e3 (2018).
80. C. Kosse, C. Schöne, E. Bracey, D. Burdakov, Orexin-driven GAD65 network of the lateral hypothalamus sets physical activity in mice. *Proc. Natl. Acad. Sci. U.S.A.* **114**, 4525–4530 (2017).
81. E. H. Nieh *et al.*, Inhibitory input from the lateral hypothalamus to the ventral tegmental area disinhibits dopamine neurons and promotes behavioral activation. *Neuron* **90**, 1286–1298 (2016).
82. M. J. McKinley *et al.*, The median preoptic nucleus: Front and centre for the regulation of body fluid, sodium, temperature, sleep and cardiovascular homeostasis. *Acta Physiol. (Oxf.)* **214**, 8–32 (2015).
83. Z. Wu, A. E. Autry, J. F. Bergan, M. Watabe-Uchida, C. G. Dulac, Galanin neurons in the medial preoptic area govern parental behaviour. *Nature* **509**, 325–330 (2014).
84. Z. D. Zhao *et al.*, A hypothalamic circuit that controls body temperature. *Proc. Natl. Acad. Sci. U.S.A.* **114**, 2042–2047 (2017).
85. T. C. Chou *et al.*, Afferents to the ventrolateral preoptic nucleus. *J. Neurosci.* **22**, 977–990 (2002).
86. S. Kodani, S. Soya, T. Sakurai, Excitation of GABAergic neurons in the bed nucleus of the stria terminalis triggers immediate transition from non-rapid eye movement sleep to wakefulness in mice. *J. Neurosci.* **37**, 7164–7176 (2017).
87. I. Gritti, L. Mainville, M. Mancia, B. E. Jones, GABAergic and other noncholinergic basal forebrain neurons, together with cholinergic neurons, project to the mesocortex and isocortex in the rat. *J. Comp. Neurol.* **383**, 163–177 (1997).
88. E. C. Harding, N. P. Franks, W. Wisden, Sleep and thermoregulation. *Curr. Opin. Physiol.* **15**, 7–13 (2020).
89. J. A. Prasad, B. J. Carroll, S. M. Sherman, Layer 5 corticofugal projections from diverse cortical areas: Variations on a pattern of thalamic and extrathalamic targets. *J. Neurosci.* **40**, 5785–5796 (2020).
90. K. Tossell *et al.*, Sleep deprivation triggers somatostatin neurons in prefrontal cortex to initiate nesting and sleep via the preoptic and lateral hypothalamus. bioRxiv [Preprint] (2020). https://doi.org/10.1101/2020.07.01.179671 (Accessed 2 July 2020).
91. V. van der Vinne *et al.*, Continuous and non-invasive thermography of mouse skin accurately describes core body temperature patterns, but not absolute core temperature. *Sci. Rep.* **10**, 20680 (2020).
92. J. Bartram *et al.*, Cortical Up states induce the selective weakening of subthreshold synaptic inputs. *Nat. Commun.* **8**, 665 (2017).